Steady-state stability and bifurcations of friction oscillators due to velocity-dependent friction characteristics

H Hetzler*, **D Schwarzer,** and **W Seemann**
Fakultät für Maschinenbau, Institut für Technische Mechanik, Universität Karlsruhe (TH), Karlsruhe, Germany

The manuscript was received on 22 May 2006 and was accepted after revision for publication on 12 October 2006.

DOI: 10.1243/14644193JMBD80

Abstract: This article presents an analytical investigation on stability and bifurcation behaviour due to an exponential and a generalized friction characteristics in the sliding domain of a simple friction oscillator, which is commonly referred to as 'mass-on-a-belt' oscillator. The friction is described by a friction coefficient which depends on the relative velocity between the two tribological partners.

The standard way of examining the steady-state only gives very rough insight in the behaviour and is not able to provide further informations about the steady-state's basin of attraction or about limit-cycles. It is found that the system may undergo bifurcations of Hopf type. Hereby, the character of the bifurcations strongly depends on the parameters of the friction characteristic.

Keywords: friction oscillator, non-linear friction characteristics, stability, bifurcation, averaging, disc-brake groan

1 MECHANICAL MODEL

1.1 Introduction

The considerations presented within this article are motivated by examinations on vehicle disc-brake vibrations. Such vibrations are usually classified with regard to their frequencies and hence to the acoustical impression on the environment. Basically, two huge classes of vibrational phenomena can be outlined: high frequency squeal and low frequency noises, often referred to as 'groan', 'muh', 'chatter' on the one hand, and 'judder' on the other hand.

Commonly, the basic mechanism behind squeal is explained by eigenvalue coupling in systems of differential equations exhibiting non-symmetric displacement proportional matrices ('stiffness-matrices'). These non-symmetric matrices may arise due to non-conservative contact-forces ('follower-forces') [**1**, **2**] or non-symmetric stiffness coupling [**3**].

Corresponding author: Fakultät für Maschinenbau, Institut für Technische Mechanik, Universität Karlsruhe (TH), Kaiserstraße 12, 76131 Karlsruhe, Germany. email: hetzler@itm.uni-karlsruhe.de

Low frequency oscillations, however, may be divided into forced vibrations ('judder') and self-excited oscillations ('groan'). While the first usually is caused by variations of the disc-thickness, the reasons of the latter are still in discussion. A comprehensive overview on brake noise can be found e.g. in reference [**2**]. Furthermore, a very profound review of friction induced vibration phenomena can be found in reference [**4**].

1.2 Experimental results

Low frequency 'groaning' noises are often explained as stick–slip vibrations. In order to investigate this theory, experimental studies have been carried out. Figure 1 shows phase diagrams of the state variables $(x, \dot{x})$ of the pad for several speeds (black). Additionally, at each pad position x, the corresponding speed v_C of the contact point on the disc is plotted (grey) – hereby periods of vanishing relative speed $v_{rel} = v_C - \dot{x}$, which is a precondition for stiction, are easily identified. It is found that the oscillations show a twofold behaviour: for almost vanishing relative speeds up to 0.5–1 cm/s large amplitudes and vanishing relative speed can be observed (1).

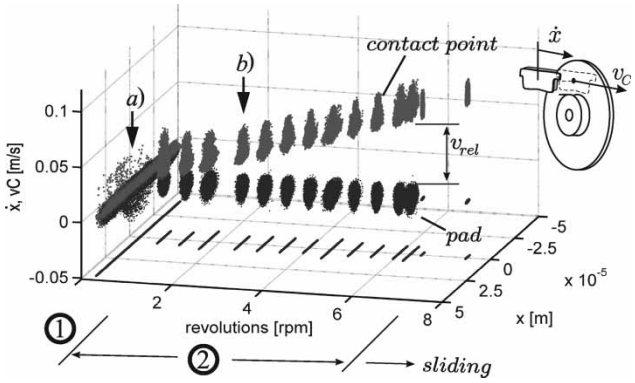

Fig. 1 State variables (x, $\dot{x}$) of the pad (black), and the corresponding speed of the contact point (x, v_C) on the disc (grey), plotted over the nominal revolution speed (min^{-1})

Therefore, in this domain the assumption of periods of stiction and hence stick–slip oscillations is plausible (see Fig. 2(a)).

However, at higher speeds (1–10 cm/s) the picture is changed (2): whereas the contact point speed v_C scales linearly with the revolution speed, the amplitudes of the pad's oscillations stay almost constant and the relative speed between disc and pad increases (see Fig. 2(b)). Here, oscillations exhibiting periods of stiction seem not very plausible and consequently besides the stick–slip mechanism another explanation has to be found. Since the experimental tests revealed a velocity-dependent friction characteristics, the influence of different friction characteristics on the behaviour of a simple one-DOF model of the brake pad will be studied in the following (Fig. 5).

1.3 Mechanical model

The mechanical model (Figs 3 and 4) consists of a lumped mass m, which is pressed onto a belt by a normal force F_B, while the belt moves at the constant speed v_0. The mass is attached to the inertial surroundings by a linear viscous damper (damping coefficient d) and a linear elasticity (stiffness c). The position of the mass is described by the coordinate x.

In addition to the inertia forces and the coupling to the inertial system, the mass is effected by the normal contact force N and the friction force R. Depending on the relative velocity between the mass and the belt, the character of R is twofold, i.e. it can represent sliding friction or stiction.

Written in the sense of Filippov, the equation of motion reads

$$\ddot{x} + 2D\omega_0\dot{x} + \omega_0^2 x \in \frac{1}{m}R,$$
$$R = \begin{cases} [-\mu_0 N;\ +\mu_0 N]\text{: } w = 0 \\ \text{sign}(w)\mu(w)N\text{: } w \neq 0 \end{cases} \quad (1)$$

with the relative velocity $w = v_0 - \dot{x}$ between block and belt, the dimensionless damping measure $D = (d/2m\omega_0)$, the natural frequency $\omega_0 = \sqrt{(c/m)}$ of the undamped system, and the normal contact force N. Depending on the relative velocity w, the right-hand side either represents sliding friction in the sense of coulomb ($w \neq 0$) or static friction as a constraint force ($w = 0$). The latter case will not be considered in the following.

1.4 Friction models

In this article, the sliding friction force is described in the sense of coulomb as being proportional to the normal contact force N, where the ratio is referred to as the friction coefficient μ. Although this coefficient depends on a huge variety of parameters, the model used in the following studies will be confined to the dependence on the relative velocity w between the mass and the belt.

1.4.1 Characteristic showing exponential decay

Motivated by the experimental observations (see Fig. 5 (a)), as a first model an exponentially decaying description of the friction characteristic was chosen

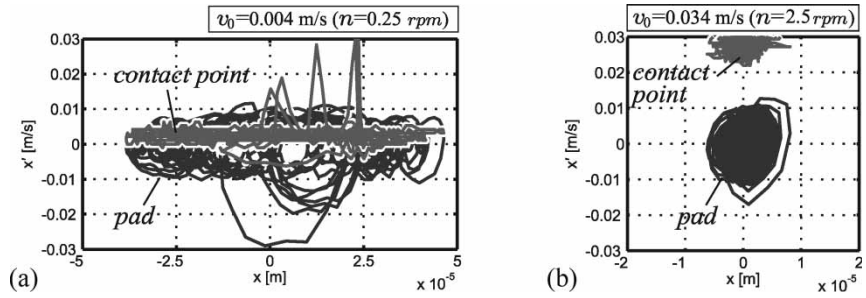

Fig. 2 Exemplary phase diagrams (x, $\dot{x}$) of the pad (black) and corresponding speed (x, v_C) of the contact point on the disc (grey): (a) nominal speed of 0.25 min^{-1} and (b) nominal speed of 2.5 min^{-1}

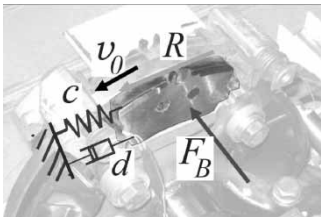

Fig. 3 Disc-brake as technical application

according to

$$\mu(w) = \mu_\infty + \Delta\mu e^{-a|w|}, \quad w = v_{\text{rel}} = \dot{x} - v_0 \tag{2}$$

with $\Delta\mu = \mu_0 - \mu_\infty$, the absolute value $|w|$ of the relative velocity, and a slope parameter a (Fig. 5). This model seems quite advantageous, since it catches the measured mean value curve of μ very good, while it only demands two parameters $\Delta\,\mu$, a [**5**].

It shall be mentioned, that expanding the exponential function into a series and truncating it after the linear term yields

$$\mu^*(w) = \mu_\infty + \frac{\Delta\mu}{1 + a|w|} \tag{3}$$

which is also a very common friction model in references [**4**] and [**6**].

The exponentially decaying friction characteristics partially resembles the well-known Stribeck curve. Since the experimental observations did not show viscous friction, the model does not include an increase of the friction coefficient at higher relative speeds.

1.4.2 Generalized characteristic

Although this latter model (3) exhibits the same stability behaviour with respect to the steady state, it does not cause bifurcations as e.g. equation (2) does; as will be seen, bifurcations of Hopf type will only occur, if the chosen friction model depends on the velocity at least cubically, giving rise to a cubical amplitude equation.

Therefore, to allow for investigations of the local bifurcation behaviour, a μ-characteristic of the pattern

$$\begin{aligned} \mu &= \mu_0 + k_1 w + k_2 w^2 + k_3 w^3, \\ w &= v_{\text{rel}} = \dot{x} - v_0 \end{aligned} \tag{4}$$

is investigated.

Of course, this model may not exhibit the same behaviour as the exponential model (2), since it represents only a polynomial of third order, whereas the exponential function needs a representation using an infinite series. However, it will be sufficient to study stability and local bifurcation behaviour.

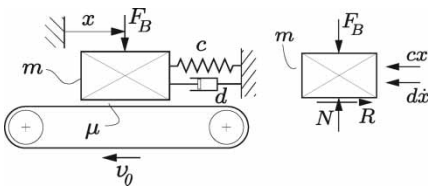

Fig. 4 Considered friction oscillator

2 STEADY STATE AND ITS LINEAR STABILITY IN THE SLIDING

Assuming the relative velocity $w > 0$, the equation of motion is given by

$$\ddot{x} + 2D\omega_0\dot{x} + \omega_0^2 x = \frac{N}{m}\mu(w) \tag{5}$$

The steady state can be calculated as

$$x_S = \frac{N}{m\omega_0^2}\mu(v_0) \tag{6}$$

In most engineering applications, only the linear stability of the steady state is considered to answer the question if self-sustained oscillations arise due to a destabilization of the steady state, or not. This is correct as long as x_S is a hyperbolic fixed-point, i.e. the linearized system has no eigenvalues with vanishing real part (theorem of Hartman/Grobman, c.f. e.g. [**7**]). To carry out a linear stability analysis, the equation of motion is linearized about the steady state and the linear variational equation for the perturbation $\Delta x = x - x_S$ is derived as

$$\Delta\ddot{x} + \underbrace{\left[2D\omega_0 + \frac{N}{m}\frac{\partial\mu(w)}{\partial w}\bigg|_{\dot{x}=0}\right]}_{=\delta}\Delta\dot{x} + \omega_0^2\Delta x = 0 \tag{7}$$

Note that $(\partial\mu(w)/\partial w)|_{\dot{x}=0}$ denotes the local gradient of the friction characteristic at the steady state $w = v_0$. This steady state is linearly stable if the system is really damped, i.e. if the extended damping term δ is positive. If it is negative, the steady state is unstable. For $\delta = 0$, the steady state is not a hyperbolic fixed-point, and therefore a stability analysis using the linearized system in principle is not allowed. In this case, a non-linear analysis will be necessary.

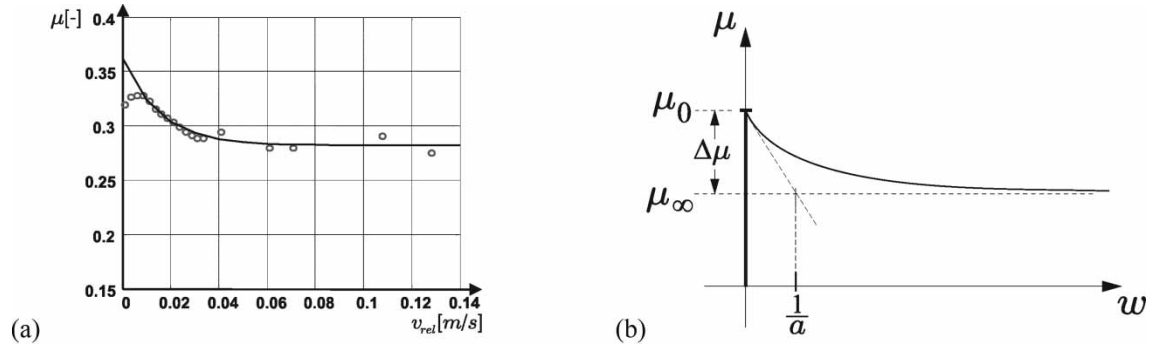

Fig. 5 (a) Measured mean values of the friction coefficient μ (circles) and corresponding exponential approximation and (b) parameters of the exponential friction model

The general condition for linear stability of the steady state is

$$x_S \text{ lin. stable} \longleftrightarrow D\omega_0 - \frac{N}{2m}\frac{\partial\mu(w)}{\partial w}\bigg|_{\dot{x}=0} > 0 \qquad (8)$$

or, more clearly

$$x_S \text{ lin. stable} \longleftrightarrow d - N\ \frac{\partial\mu(w)}{\partial w}\bigg|_{\dot{x}=0} > 0 \qquad (9)$$

Obviously, the linear stability of the steady state only depends on the damping d and on the properties of the friction force, but not on the stiffness c (resp. natural frequency ω_0) of the system.

3 EXPONENTIALLY DECAYING CHARACTERISTIC

3.1 Analytical approximative solution for periodic sliding motion

3.1.1 Amplitude equation by first-order averaging

Assuming only weakly non-linear behaviour that develops on two different timescales – on the fast scale the oscillation and the amplitude growth on the slow scale – it seems promising to use an averaging method to find approximate solutions. Here, a first-order method is used, which is also known as the method of slow phase and amplitude [**8**]. Introducing the coordinate shift $z = x - x_S$ (i.e. $\dot{z} = \dot{x}, \ldots$) into the equation of motion (5), inserting the exponential friction model and arranging in standard-form yields

$$\begin{aligned}\ddot{z} + \omega_0^2 z &= -2D\omega_0\dot{z} + \frac{N\Delta\mu}{m}\left(\mathrm{e}^{-a(v_0-\dot{z})} - \mathrm{e}^{-av_0}\right)\\ &= -2D\omega_0\dot{z} + \frac{N\Delta\mu}{m}\mathrm{e}^{-av_0}(\mathrm{e}^{+a\dot{z}} - 1) \qquad (10)\end{aligned}$$

Scaling to the dimensionless time $\tau = \omega_0 t$ and introduction of the dimensionless coordinates

$$L = \frac{N}{c}, \quad \alpha = a\omega_0 L, \quad V_0 = \frac{v_0}{\omega_0 L}, \quad \gamma = \Delta\mu\mathrm{e}^{-\alpha V_0}$$

allows to write equation (10) as

$$\zeta'' + \zeta = -2D\zeta' + \gamma(\mathrm{e}^{\alpha\zeta'} - 1) \qquad (11)$$

where $\zeta = z/L$ is a dimensionless position coordinate and $()' = (\mathrm{d}/\mathrm{d}\tau)$ denotes differentiation with respect to the dimensionless time τ.

This equation is transformed to new coordinates A, θ ($A \geqslant 0$, $\theta \in [0, 2\pi)$), which are referred to as amplitude and phase. Introducing the transformations and abbreviations

$$\zeta = A(\tau)\sin\theta(\tau) = AS, \quad \theta(\tau) = \tau + \psi(\tau) \qquad (12)$$

$$\zeta' = A(\tau)\cos\theta(\tau) = AC \qquad (13)$$

into equation (11), the right-hand side reads ($\varepsilon \ll 1$)

$$\varepsilon f(\zeta, \zeta') = -2DAC + \gamma(\mathrm{e}^{\alpha A\zeta'} - 1) \qquad (14)$$

Averaging over one period yields the amplitude equation

$$A' = \frac{1}{2\pi}\int_{\theta=0}^{2\pi} f(\zeta, \zeta')\cos\theta\,\mathrm{d}\theta \qquad (15)$$

$$= -\frac{D}{\pi}A\langle C^2\rangle + \frac{\gamma}{2\pi}\left[\langle\mathrm{e}^{\alpha AC}C\rangle - \langle C\rangle\right] \qquad (16)$$

where $\langle g\rangle = \int_{\theta=0}^{2\pi} g\,\mathrm{d}\theta$ denotes 2π-times the average of the function g over one period. To calculate this latter average, equation (16) is rewritten using a series representation of the exponential function,

yielding

$$A' = -\frac{D}{\pi}A\langle C^2\rangle + \frac{\gamma}{2\pi}\left[\int_0^{2\pi}\sum_{n=1}^{\infty}\frac{\alpha^n C^n}{n!}C\,\mathrm{d}\theta - \langle C\rangle\right] \quad (17)$$

Uniform convergence of the integrand (criterion of Weierstrass) allows swapping of integration and summation. Motivated by $\langle C^{2n+1}\rangle = 0$ ($n \in \mathbb{N}$) indices are reset, yielding the amplitude equation

$$A' = -DA + \gamma\sum_{k=1}^{\infty}\frac{\alpha^{2k-1}}{(2k-1)!}\frac{\langle C^{2k}\rangle}{2\pi}A^{2k-1} \quad (18)$$

Since the right-hand side of equation (14) together with equations (12) and (13) does not contain any sine-terms, the corresponding average vanishes and therefore the phase speed keeps constantly zero

$$\psi' = -\frac{1}{2\pi A}\int_{\theta=0}^{2\pi} f(\zeta, \zeta')\sin\theta\,\mathrm{d}\theta = 0 \quad (19)$$

3.1.2 Fixed-points and limit-cycles

To find fixed-points or limit-cycles, equation (18) is investigated for stationary amplitudes $\dot{A} = 0$. After that, the stability of these amplitudes is studied.

From equation (18), it follows that

$$A_1 = 0 \quad (20)$$

is always a possible stationary amplitude. Separating this solution from equation (18) yields

$$\begin{aligned} 0 &= -D + \gamma\sum_{k=1}^{\infty}\frac{a^{2k-1}}{(2k-1)!}\frac{\langle C^{2k}\rangle}{2\pi}A^{2k-2} \\ &= -D + \gamma\left[\frac{\alpha}{2} + \sum_{k=2}^{\infty}\frac{a^{2k-1}}{(2k-1)!}\frac{\langle C^{2k}\rangle}{2\pi}A^{2k-2}\right] \end{aligned}$$

and hence

$$2D - \gamma\alpha = 2\gamma\sum_{k=2}^{\infty}\frac{a^{2k-1}}{(2k-1)!}\frac{\langle C^{2k}\rangle}{2\pi}A^{2k-2} \quad (21)$$

Since γ and the quantities in the sum are positive, equation (21) can only hold for real, positive amplitudes A, if the difference of the left-hand side is positive. A limit cycle with a real amplitude can only exist if

$$A_2 \in \mathbb{R}^+ \longleftrightarrow 2D - \gamma\alpha \overset{!}{>} 0 \quad \text{(bifurcation)} \quad (22)$$

Equation (22) denotes a bifurcation, since the system's steady-state solution may be surrounded by a limit cycle or not. Resubstitution of the dimension-carrying quantities shows that this latter equation corresponds to the condition of linear stability, equation (8). Hence, the bifurcation border only depends on the damping d and on properties of the friction, but is independent of the system's stiffness.

3.1.3 Validity domain of the approximations

Equation (11) holds for $\zeta' < V_0$, i.e. in the entire half plane of sliding motion below the stiction line. Owing to the harmonic ansatz, the presented considerations will only be valid as long as the trajectories do not touch the stiction line – since this would lead to the stick–slip limit cycle. Therefore, the examined motions are confined to the section denoted by Σ_0 (see Fig. 6), which is centred about ($\zeta = 0$, $\zeta' = 0$) and for weak non-linearities approximately of a circular shape. By geometrical considerations, the radius of this circular area is given by $r = V_0$. Hence, a limit-cycle in the sense of equation (22) will only exist if

$$A_2 \overset{!}{<} V_0 \quad \text{(validity of solution ansatz)} \quad (23)$$

is fulfilled (e.g. trajectory γ_0 in Fig. 6).

3.2 Stability of fixed-points and limit-cycles

To study the stability of the stationary amplitudes given by equations (20) and (21), the first derivatives of equation (18) with respect to A are examined

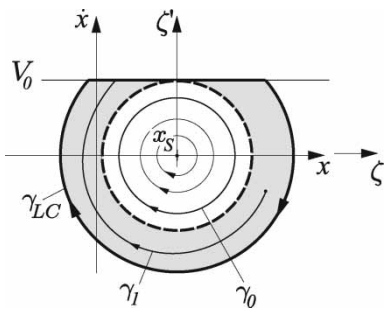

Fig. 6 Qualitative set-up of the phaseplane ($D = 0$)

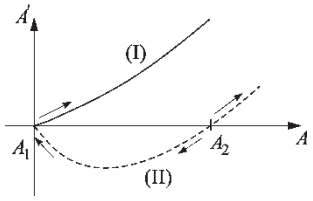

Fig. 7 Qualitative sketch of the amplitude growth behaviour and stability

(see Fig. 7). Carrying out the derivations yields

$$\frac{\mathrm{d}A'}{\mathrm{d}A} = -D + \gamma \sum_{k=1}^{\infty} \frac{\alpha^{2k-1}}{(2k-1)!} \frac{\langle C \rangle}{2\pi} (2k-1) A^{2k-2} \tag{24}$$

$$= -D + \gamma \left[\frac{\alpha}{2} + \sum_{k=2}^{\infty} \frac{\alpha^{2k-1}}{(2k-2)!} \frac{\langle C \rangle}{2\pi} A^{2k-2} \right] \tag{25}$$

Evaluation at the fixed-point $A_1 = 0$ yields

$$\left. \frac{\mathrm{d}A'}{\mathrm{d}A} \right|_{A=A_1} = -D + \gamma \frac{\alpha}{2} \tag{26}$$

As qualitatively sketched in Fig. 8, two cases can be outlined.

1. $(\mathrm{d}A'/\mathrm{d}A)|_{A=A_1} > 0$: the steady-state fixed-point is unstable. Simultaneously, condition (22) assuring the existence of the cycle is not fulfilled – hence there is only an unstable fixed-point.
2. $(\mathrm{d}A'/\mathrm{d}A)|_{A=A_1} < 0$: the steady-state fixed-point is stable and at the same time, condition (22) is fulfilled. Hence, there is an unstable limit cycle of amplitude A_2 coexisting to the stable fixed-point. The instability of the limit-cycle can easily be seen from Fig. 7, since small perturbations will be amplified. Hence, there are a stable fixed-point and an unstable limit-cycle (Fig. 8). The amplitude A_2 of the unstable limit-cycle has to fulfill the limit condition (23) to avoid being catched by the stick–slip limit cycle.

Hence, the system undergoes a sub-critical Hopf-bifurcation between (1) and (2): unstable fixed-point $\leftrightarrow$ stable fixed-point + unstable limit cycle (see Fig. 8). For a formal proof see reference [**9**].

3.2.1 Parameter discussion

Equation (22) shows that the bifurcation behaviour mainly depends on the damping measure D and the shape parameter α. With the help of the function

$$f(D, \alpha) = 2D - \gamma\alpha \tag{27}$$

illustrated in Fig. 9, a picture of the different possible phase plots is given. Corresponding to equation (22), the bifurcation point of the Hopf-bifurcation can be implicitly written as $f(D, \alpha) = 0$, which is illustrated in Fig. 9 as a black solid contour line labelled with 'cond. 2'.

An eigenvalue analysis of the linearized system yields two more conditions describing the change of the topological structure in the phase plot in a closed region about the fixed-point, where the fixed-point changes from a saddle node over a degenerated node to a spiral and vice versa (for more details see reference [**10**]). These conditions are (see the white solid lines in Fig. 9)

$$\begin{aligned} &\text{'cond. 1'}: \; f(D, \alpha) = -2 \\ &\text{'cond. 4'}: \; f(D, \alpha) = 2 \end{aligned} \tag{28}$$

The dashed contour line labelled with 'cond. 3' corresponds to equation (23), where the limit-cycle vanishes because of touching the stick–slip limit

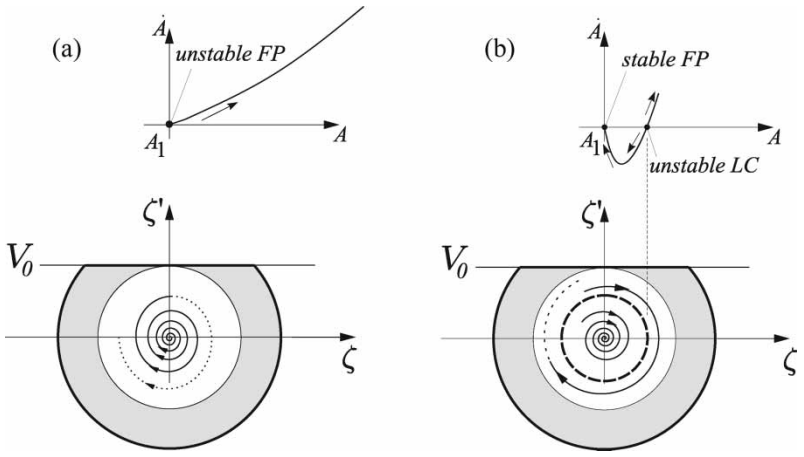

Fig. 8 Amplitude growth and phase plot. (a) unstable fixed-point and (b) stable fixed-point and unstable limit cycle

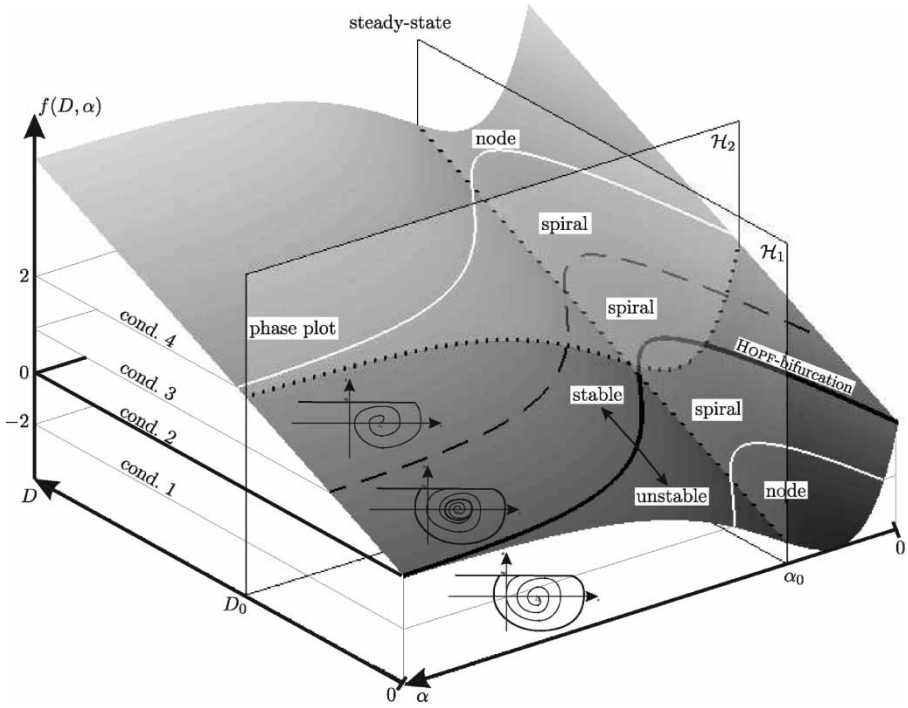

Fig. 9 Parameter discussion

cycle. With the help of these contour lines, it is possible to evaluate the behaviour of the examined system for given parameters D and α.

To allow for a better overview, section planes where a single parameter is kept constant can be displayed. For example, Fig. 10 shows the result for $\mathcal{H}_1$ ($\alpha = \text{const}$).

3.3 Numerical simulations

To verify the derived behaviour of the simple one-DOF friction oscillator with an exponentially decaying friction characteristic, numerical simulations were carried out using the explicit variable time-step Runge–Kutta–Fehlberg scheme of order 4(5) provided by MATLAB (ODE45). The values for the parameters were chosen according to the examined disc-brake model:

normal force	$N = 9000$ N
mass	$m = 1$ kg
natural frequency	$\omega_0 = 5000$ rad/s
velocitiy of the belt	$v_0 = 1$ m/s
friction coefficient	$\mu_\infty = 0.25$
difference of friction coefficients	$\Delta\mu = 0.15$
slope parameter	$a = 2$ m/s

Starting the numerical simulations with the dimensionless damping coefficient $D = 0.03$ (Fig. 11(a)), the obtained phase plot $(x, \dot{x})$ of the system shows an instable steady-state surrounded by the stick–slip limit cycle. After passing the bifurcation border $D = (1/2)\gamma\alpha = 0.036\,54$, the stability of the steady state changes to stable and an instable limit cycle is born, whose amplitude A extends by increasing the parameter D (e.g. $D = 0.04$, Fig. 11(b)). This behaviour agrees with the results received analytically in this chapter.

4 GENERALIZED FRICTION CHARACTERISTICS

4.1 Analytical approximation of periodic solutions in the sliding domain

To allow for more general studies of sliding friction influence on the bifurcation, the friction characteristics is modelled according to equation (4) as

$$\mu = \mu_0 + k_1 w + k_2 w^2 + k_3 w^3, \quad w > 0 \tag{29}$$

For example, series expansion and truncation of the exponentially decaying characteristics (2) yields

$$\mu = \mu_0 + \Delta\mu\left(-aw + \frac{a^2}{2}w^2 - \frac{a^3}{6}w^3\right) \tag{30}$$

Another very common friction characteristics is

$$\mu = \mu_0 + \Delta\mu\left(-\frac{3}{2v_m}w + \frac{1}{2v_m^3}w^3\right) \tag{31}$$

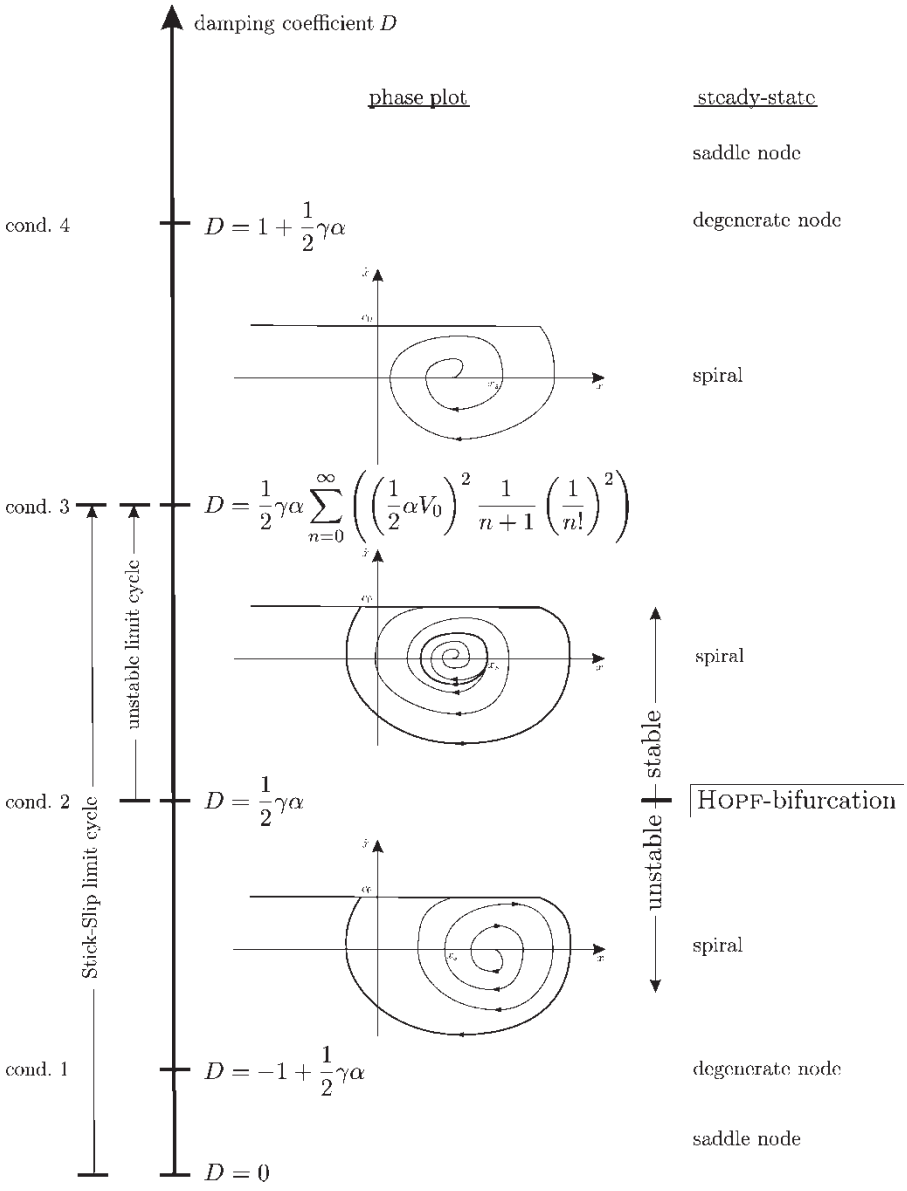

Fig. 10 Variation of D for a constant value of α: possible behaviour of the steady-state and the resulting phase plots

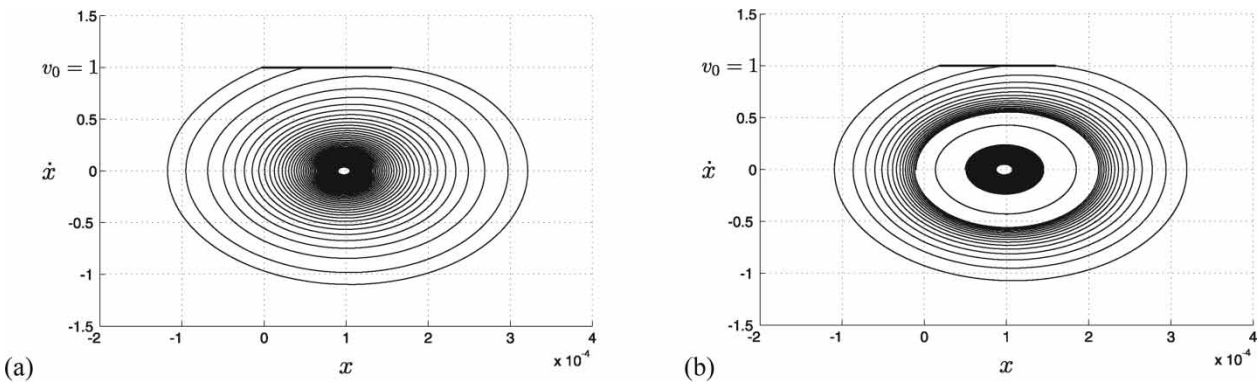

Fig. 11 Numerical simulations: (a) with $D = 0.03$ and (b) with $D = 0.04$

describing friction with a viscous influence (see reference [**11**]).

With $w = v_0 - \dot{z} \overset{!}{>} 0$, the equation of motion in standard form for averaging reads

$$\ddot{z} + \omega_0^2 z = -\mathcal{K}_1^* \dot{z} - \mathcal{K}_2^* \dot{z}^2 - \mathcal{K}_3^* \dot{z}^3 \tag{32}$$

Introducing the dimensionless

time: $\tau = \omega_0 t \quad (\text{hence}()^{\cdot} = \omega_0 ()')$

coordinate: $\zeta = \dfrac{1}{L} z \quad$ and

parameters:

$$L = \frac{N}{c}, \quad V_0 = \frac{v_0}{\omega_0 L},$$
$$\kappa_1 = L\omega_0 k_1, \quad \kappa_2 = L^2 \omega_0^2 k_2, \quad \kappa_3 = L^3 \omega_0^3 k_3$$

equation (32) reads

$$\zeta'' + \zeta = -\mathcal{K}_1 \zeta' - \mathcal{K}_2 \zeta'^2 - \mathcal{K}_3 \zeta'^3 \tag{33}$$

where

$$\mathcal{K}_1 = 2D + \kappa_1 + 2\kappa_2 V_0 + 3\kappa_3 V_0^2$$
$$\mathcal{K}_2 = -\kappa_2 - 3\kappa_3 V_0$$
$$\mathcal{K}_3 = \kappa_3$$

Proceeding in analogy to paragraph 3, first-order averaging of equation (33) yields the amplitude equation

$$A' = -\frac{1}{2}\mathcal{K}_1 A - \frac{3}{8}\mathcal{K}_3 A^3 \tag{34}$$

Equation (34) only holds if stiction will not occur, i.e.

$$\max\{\zeta'\} = A < V_0 \quad (\text{validity of Ansatz}) \tag{35}$$

Again it is found that quadratic velocity terms drop due to $\langle \cos^2\theta \cos\theta \rangle = 0$ and therefore, $\mathcal{K}_2$ has no influence on the amplitude behaviour.

4.2 Sliding steady state and limit cycles

The stationary amplitudes are given by

$$A_1 = 0 \quad \text{and} \quad A_2 = \sqrt{-\frac{4}{3}\frac{\mathcal{K}_1}{\mathcal{K}_3}} \tag{36}$$

Here, the second equation will only yield a limit cycle of real amplitude A_2, if $(\mathcal{K}_1/\mathcal{K}_3) < 0$

$$\frac{\mathcal{K}_1}{\mathcal{K}_3} < 0 \longleftrightarrow A_2 \in \mathbb{R}^+ \tag{37}$$

Hence, the existence of a limit cycle of real valued amplitude A_2 is tied to

$$\mathcal{K}_1 \mathcal{K}_3 < 0 \tag{38}$$

In implicit form, the bifurcation border is given by

$$\mathcal{K}_1 = 0 \tag{39}$$

Once again, the stability of the stationary solutions $A_{1,2}$ can be judged by looking at the slope of the amplitude equation

$$\left.\frac{\partial A'}{\partial A}\right|_{A=A_{1,2}} = -\frac{1}{2}\mathcal{K}_1 - \frac{9}{8}\mathcal{K}_3 A^2 \tag{40}$$

From equation (36), the slope for each stationary solution is found as

$$A_1\text{:}\ \left.\frac{\partial A'}{\partial A}\right|_{A=A_1} = -\frac{\mathcal{K}_1}{2}, \quad A_2\text{:}\ \left.\frac{\partial A'}{\partial A}\right|_{A=A_2} = \mathcal{K}_1 \tag{41}$$

where a negative slope denotes a stable and a positive slope an unstable amplitude A_i Considering equation (38), it can be stated that the stability is entirely determined by $\mathcal{K}_1$, whereas the existence of a limit cycle about the steady state is reigned by the quotient $\mathcal{K}_1/\mathcal{K}_3$.

While the slope of A' at $A_1 = 0$ is entirely determined by $\mathcal{K}_1$, the curvature

$$\frac{\partial^2 A'}{\partial A^2} = -\frac{9}{4}\mathcal{K}_3 A \tag{42}$$

is solely given by $\mathcal{K}_3$. Figure 13 displays the qualitative amplitude growth behaviour, depending on the slope parameter $\mathcal{K}_1$ and the curvature parameter $\mathcal{K}_3$. The sketch confirmes the analytically found stability criteria as well as the content of Fig. 12.

It has to be stressed that in above considerations, the influence of the stick–slip limit cycle had not been taken into account.

4.3 Bifurcation behaviour

As shown above, the system will undergo Hopf-bifurcations at (Fig. 14)

$$\mathcal{K}_1 = 0 \tag{43}$$

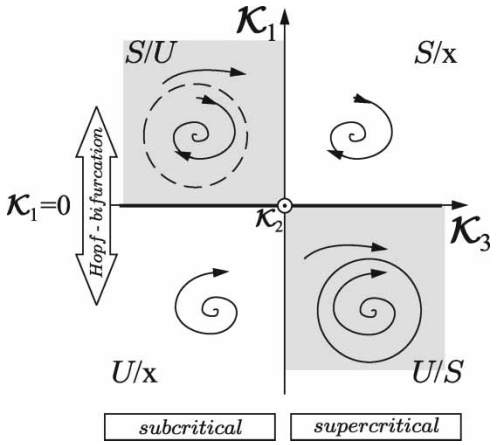

Fig. 12 Overview of the local stability and bifurcation behaviour due to equations (22) and (38), without consideration of the influence of the stick–slip limit cycle. Depending on $\mathcal{K}_{1,3}$, the resulting phase portrait is sketched. The letter combination encode the behaviour (steady-state stability/limit-cycle behaviour): U – unstable, S – stable, x – no limit cycle

This was found using a harmonic ansatz, which is only valid within a certain domain of the phase-plane; if it touches the stick–slip limit cycle, new behaviour arises. Considering equation (35), the found limit-cycle amplitudes will only hold if

$$A_2 = \sqrt{-\frac{4}{3}\frac{\mathcal{K}_1}{\mathcal{K}_3}} < V_0 \tag{44}$$

Depending on the sign of $\mathcal{K}_1$ and $\mathcal{K}_3$, two conditions assuring the limit cycle not to touch the stick–slip limit cycle can be found (see Fig. 15)

$$\mathcal{K}_1 > 0 \wedge \mathcal{K}_3 < 0\text{:} \quad \mathcal{K}_3 < -\frac{4}{3V_0^2}\mathcal{K}_1 \tag{45}$$

$$\mathcal{K}_1 < 0 \wedge \mathcal{K}_3 > 0\text{:} \quad \mathcal{K}_3 > -\frac{4}{3V_0^2}\mathcal{K}_2 \tag{46}$$

The corresponding border is denoted as $\mathcal{B}_1$.

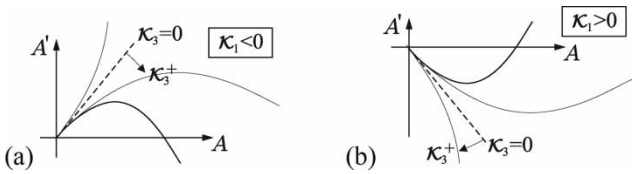

Fig. 13 Influence of $\mathcal{K}_1$ and $\mathcal{K}_3$ on the amplitude growth A' behaviour: $\mathcal{K}_1$ gives the slope at $A = 0$ and $\mathcal{K}_3$ determines the curvature of A'

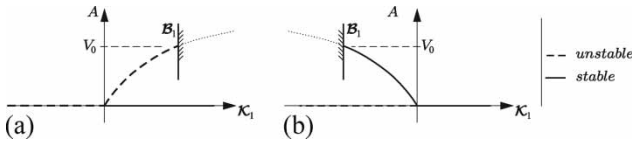

Fig. 14 Bifurcation diagrams. At $\mathcal{B}_1$ the solution is catched by the stick–slip limit-cycle: a) subcritical Hopf-bifurcation and b) supercritical Hopf-bifurcation

Since these conditions are independent of $\mathcal{K}_2$, the latter can be interpreted as a free parameter, spanning planes in the ($\mathcal{K}_1$, $\mathcal{K}_2$, $\mathcal{K}_3$) space.

In the second quadrant of the $\mathcal{K}_1$, $\mathcal{K}_3$ section, the limit cycle A_2 will only exist on the right of $\mathcal{B}_1$, in the fourth quadrant only left of it ($\mathcal{K}_2 \in \mathbb{R}$). In the acute-angled regions between $\mathcal{B}_1$ and $\mathcal{B}_2$, A_2 does no longer denote the amplitude of a limit-cycle; however, it still gives the border of regions of different growth behaviour in sliding motion. The bordering plane $\mathcal{B}_2$ marks the limit, where A_2 trespasses the stick–slip limit cycle; due to its complexity, this case will not be considered in the following (case (x) in Fig. 15).

As an example, phase-portrait no. (3) in Fig. 15 outlines a flow that diverges from the dashed circle. Here, the actual separatrix between the basin of the steady state and that of the stick–slip limit cycle is given by the limit trajectory that just reaches the stick–slip limit cycle in its point of maximum velocity. This border is only outlined qualitatively here.

When trespassing the $\mathcal{K}_1 = 0$ iso-plane, the system undergoes a Hopf-bifurcation, whose specific type depends on the sign of $\mathcal{K}_3$; for $\mathcal{K}_3 > 0$ the bifurcation will be supercritical, for $\mathcal{K}_3 < 0$ it will be subcritical.

4.4 Influence of the friction parameters on the local behaviour

Since $\mathcal{K}_i$ ($i = 1, 2, 3$) are the coefficients in the standard averaging form and do not represent the physical parameters of the friction curve, further discussion should rather be in terms of κ_j ($j = 1, 2, 3$).

If K is the space of coefficients $\mathcal{K}_i$ and P the space of physical parameters κ_j, the equations (34) represent a mapping M: $\kappa_1 \times \kappa_2 \times \kappa_3 \rightarrow \mathcal{K}_1 \times \mathcal{K}_2 \times \mathcal{K}_3$,

$$k = M\kappa + d, \quad k \in K, \kappa \in P \tag{47}$$

Here, k represents a set of coefficients in the averaging equation and κ is a set of friction curve parameters. Since M is linear and invertible (det $M \neq 0$), a plane will be mapped onto a plane and a point to a point. The system's damping is included in the offset d.

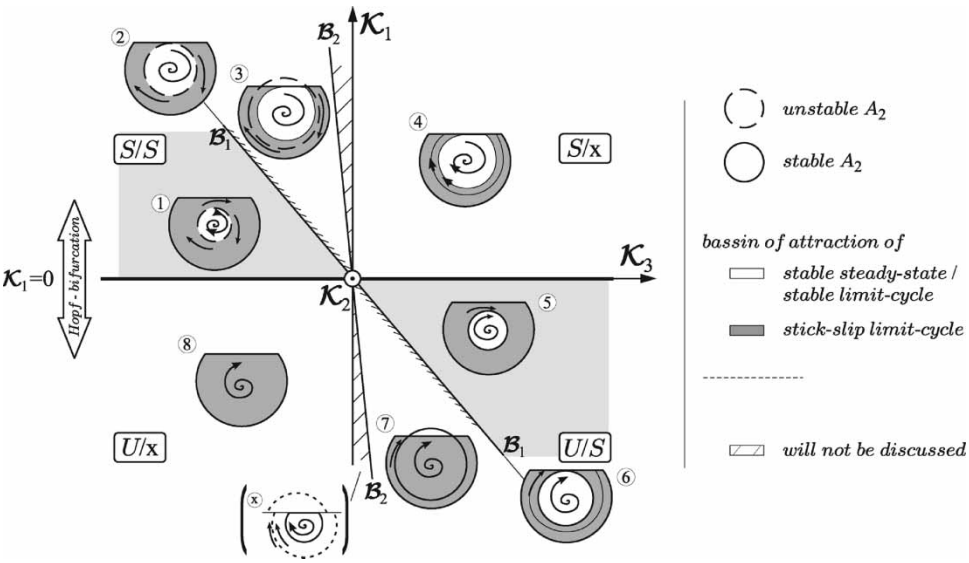

Fig. 15 Overview on the global behaviour of the phase-portrait

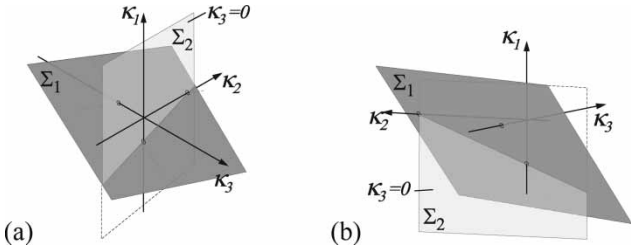

Fig. 16 Bifurcation border $\Sigma_1 = 0$ and isoplane $\Sigma_2 = 0$ in the space of the physical friction parameters

Hence, the bifurcation border $\mathcal{K}_1 = 0$ and the isoplane $\mathcal{K}_3 = 0$ in K transform into P as

$$\mathcal{K}_1 = 0 \longrightarrow \Sigma_1 = \Sigma_1(\kappa) = 0 \tag{48}$$

$$\mathcal{K}_3 = 0 \longrightarrow \Sigma_2 = \Sigma_2(\kappa) = 0 \tag{49}$$

In the sense of a Hessian normal form, $\Sigma_1(\kappa) = \delta$ yields the distance δ between κ and the plane $\Sigma_1 = 0$. It is $\delta > 0$ if κ and the origin $(0, 0, 0)^{\mathrm{T}}$ are on the same side of the plane, whereas $\delta < 0$ holds

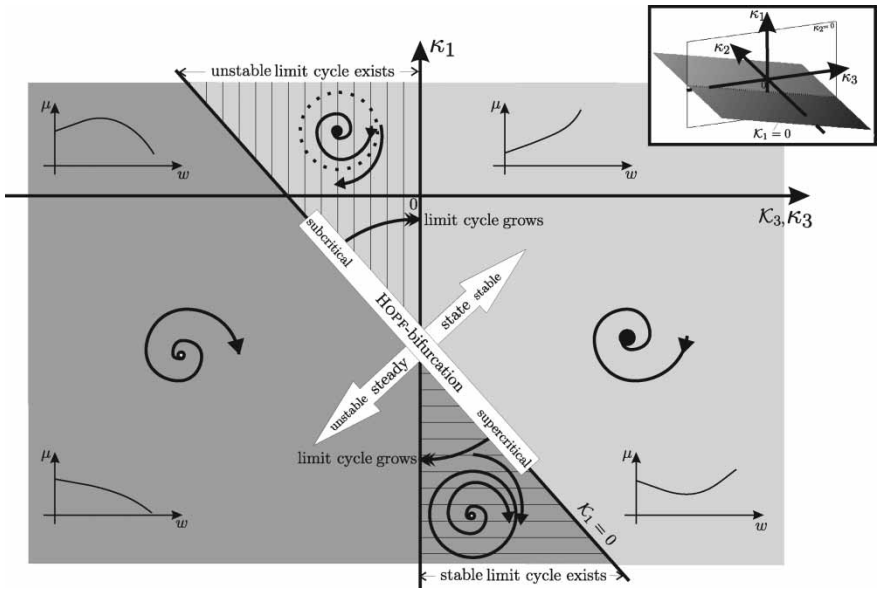

Fig. 17 Section of the parameter space P: influence of friction curve parameters κ_1, κ_3 ($\kappa_2 = 0$) **[12]**

if they are on opposite sides. Figure 16 outlines exemplarily the bifurcation plane Σ_1 in the (κ_1, κ_2, κ_3) parameter space for a physically damped system (i.e. $D \in [0, 1)$).

Parameter triples κ evoking a stable steady state (i.e. $\mathcal{K}_1 > 1$ and hence $\delta = \Sigma_1(\kappa) > 0$) are to be found 'above' Σ_1 in Fig. 16(a), whereas κ belonging to unstable steady states are situated 'below' this plane (Fig. 16(b)).

Due to equation (38), limit cycles about the steady state will only exist, if $\mathcal{K}_1$ and $\mathcal{K}_3$ have opposite signs. Hence, limit cycle will only exist in the acute-angled wegde-shaped space between Σ_1 and Σ_2.

The bordering planes $\mathcal{B}_1$ and $\mathcal{B}_2$ can be displayed in K in the same manner, but for clarity's sake, they are not included in Fig. 16.

Concluding, Fig. 17 shows a section of the three-dimensional parameter space P at $\kappa_2 = 0$.

5 CONCLUSION

Usually, the stability of the classical friction oscillator is studied by only linearizing the equations of motion about the steady state and examination of the eigenvalues. This article revises the stability in the vicinity of the sliding steady state for several friction characteristics. The focus is set on an exponentially decaying characteristics, which is motivated by experimental observations. As a generalization, a polynomial characteristics of third order is examined to study the bifurcation behaviour in more detail.

By means of an averaging method of first order, it is found that the transition behaviour between stable and unstable states of sliding motion is more complex than suggested by the classical stability analysis and involves bifurcations of Hopf type. The special type of bifurcation (sub- or supercritical) depends on the parameters of the friction curve.

REFERENCES

1 **von Wagner, U., Jearsiripongkul, T., Vomstein T., Chakraborty, G.,** and **Hagedorn, P.** Brake squeal: modeling and experiments. *VDI-Ber.*, 2003, **1749**, 173–186.

2 **Wallaschek, J., Hach, K.-H., Stolz, U.,** and **Mody, P.** A survey of the present state of friction modelling in the analytical and numerical investigation of brake noise generation. In Proceedings of the ASME Vibration Conference, Las Vegas, 1999.

3 **Hoffmann, N.** and **Gaul, L.** Effects of damping on mode-coupling instability in friction induced. *ZAMM*, 2003, **83**(8), 524–534.

4 **Ibrahim, R. A.** and **Rivin, E.** Friction-induced vibration, part I. *Appl. Mech. Rev.*, 1994, **47**(7), 207–226.

5 **Hetzler, H., Seemann, W.,** and **Schwarzer, D.** Analytical investigations of Hopf-bifurcations occuring in a 1-DOF sliding-friction oscillator with application to disc-brake vibrations. In Proceedings of IDETC'05, Long Beach, 2005, DETC2005-84312, ASME 2005.

6 **Kauderer, H.** *Nichtlineare Mechanik*, 1958 (Springer-Verlag, Berlin, Göttingen, Heidelberg).

7 **Guckenheimer, J.** and **Holmes, Ph.** *Nonlinear oscillations, dynamical systems, and bifurcations of vector fields*, 1983 (Springer-Verlag, New York).

8 **Hagedorn, P.** *Non-linear oscillations*, 1988 (Clarendon Press, Oxford).

9 **Hetzler, H., Schwarzer, D.,** and **Seemann, W.** Analytical investigation of steady-state stability and Hopf-bifurcations occurring in sliding friction oscillators with application to low-frequency disc brake noise. In *Communications in nonlinear science and numerical simulation (CNSNS)*, 2006 (Elsevier, Amsterdam).

10 **Strogatz, S. H.** *Nonlinear dynamics and chaos*, 2000 (Westview Press, Cambridge).

11 **Fidlin, A.** *Nonlinear oscillations in mechanical engineering*, 2006 (Springer-Verlag, Berlin, Heidelberg, and New York).

12 **Schwarzer, D., Hetzler, H.,** and **Seemann, H.** Bifurcation behavior of a 1-DOF sliding friction oscillator. *PAMM*, 2006, **6**(1), 331–332.

APPENDIX

Notation

a, α	slope parameter of the exponential friction characteristic (with, without dimension)
A	amplitude
c	stiffness of linear elasticity
C	abbreviation for cos θ
d	damping coefficient
D	dimensionless damping measure
F_B	normal force
k_i, κ_i	parameters of the generalized friction characteristic (with, without dimension)
$\mathcal{K}_i^*$, $\mathcal{K}_i$	abbreviations (with, without dimension)
L	characteristic length
m	mass
N	normal contact force
R	friction force
S	abbreviation for sin θ
t, τ	time (with, without dimension)
v_0,V_0	velocity of the belt (with, without dimension)
v_C	velocity of the contact point on the disc
v_m	parameter of the friction characteristic in reference [**11**]
w	relative velocity
x, ζ	coordinate of the position of the mass (with, without dimension)
γ	abbreviation

δ	extended damping term
θ	phase
μ	friction coefficient
μ_0	friction coefficient at vanishing relative velocity $w = 0$
μ_∞	friction coefficient for infinite relative velocity $w \to \infty$
Δ_μ	difference between μ_0 and μ_∞
ψ	difference of phases
ω_0	natural frequency